1 Supplementary Figures S1-S6
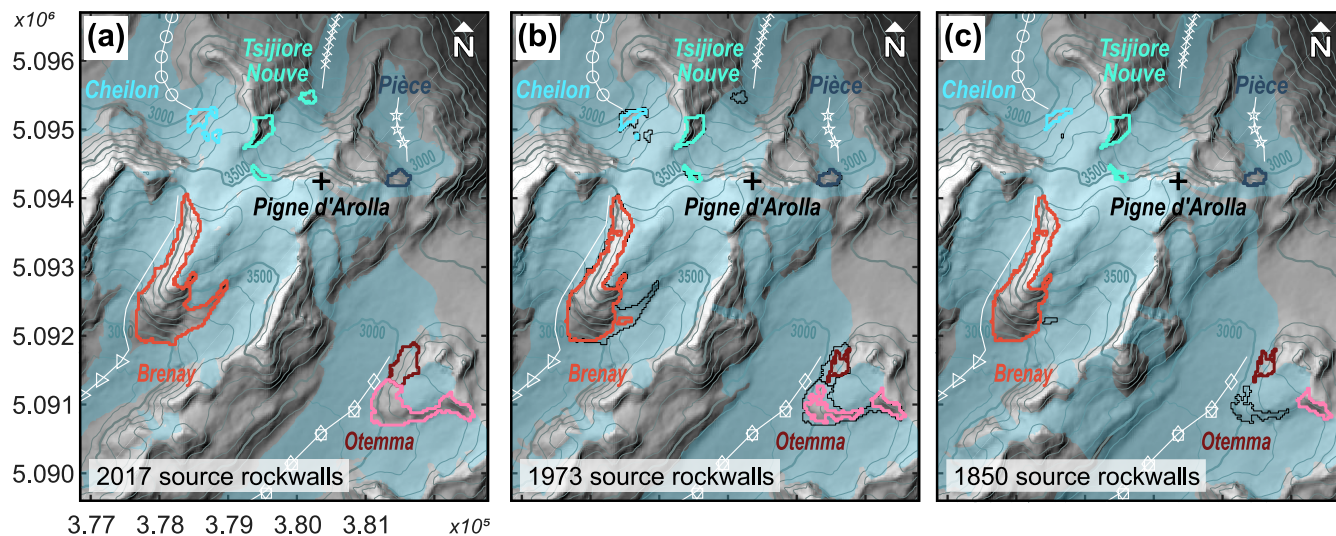
Figure S1: Hillshade images with elevation as greyshade (bright = high) outlining the studied ice-free source rockwalls around Pigne d'Arolla for the three time slices (a) 2017, (b) 1973, and (c) 1850. To visualise the temporal changes in ice cover across the debris source areas, source rockwall outlines of the year shown are coloured and underlain by the source rockwall outlines of the next younger time slice in black. Contour lines are spaced by 100 m and based on the recent DEM and, therefore, on the glacier body itself only valid for the most recent time slice. For reference, the glacier extents (blue shade), medial moraine profiles (white lines) and 2019 sample locations (white symbols) of Glacier du Brenay, Glacier de Cheilon, Glacier d'Otemma, Glacier de Pièce and Glacier de Tsijiore Nouve are indicated (glacier extents of 2016, 1973 and 1850 by Linsbauer et al., 2021, Müller et al., 1976, Maisch et al., 2000).
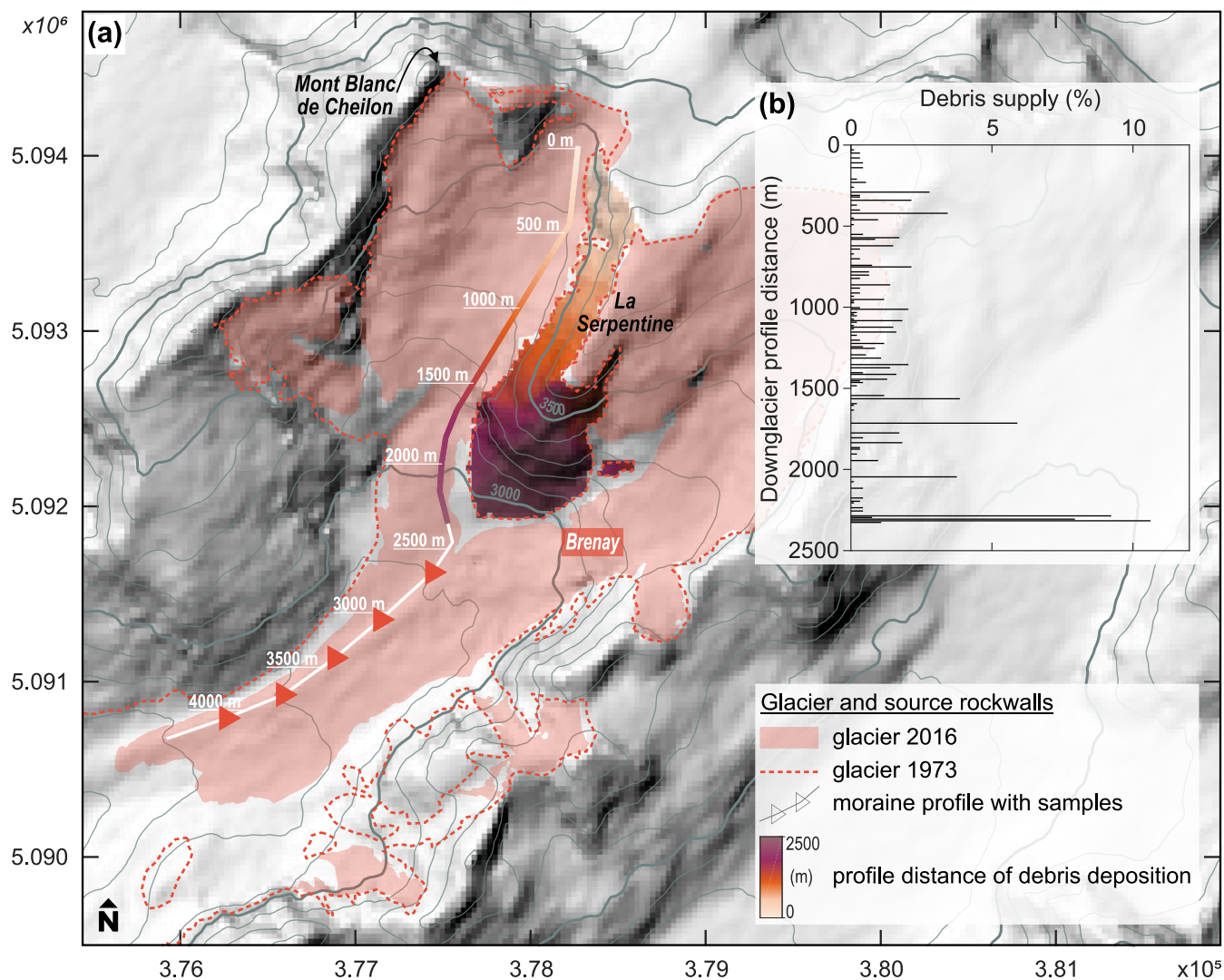
Figure S2: Weighted debris supply/deposition along the modelled medial moraine profile of Glacier du Brenay from ice-free source rockwalls of La Serpentine in 1973. (a) Hillshade image with elevation as greyshade (bright = high) showing that, due to the elongated nature of La Serpentine, debris deposition does not occur at a single confined location but along the first ~2.3 km of the modelled downglacier medial moraine profile. Therefore, at a sample location in 2019, trajectories of several debris particles will meet that were deposited at different profile distances and that experienced different transport times and exposures to cosmic radiation (see Fig. S3). The colour gradient along the downglacier profile and across the source rockwall area indicates at which downglacier profile distance a rockwall/DEM pixel supplies a debris particle, according to the flow directions of the steepest decent. Contour lines on the grid are spaced by 100 m. For reference, the 2016 and 1973 glacier extents, the medial moraine profile with downglacier distances and the 2019 sample locations are indicated (glacier extents by Linsbauer et al., 2021, Müller et al., 1976). (b) Inset aligning to the downglacier profile in (a) and showing the percentage debris particle supply along the first ~2.3 km profile distance, weighted by to the overlying rockwall area. Assuming a constant erosion rate across La Serpentine, debris supply/deposition is relatively higher where more rockwall area towers above the ice and, thus, those trajectories are more represented, when estimating an average sample age based on all modelled trajectories.
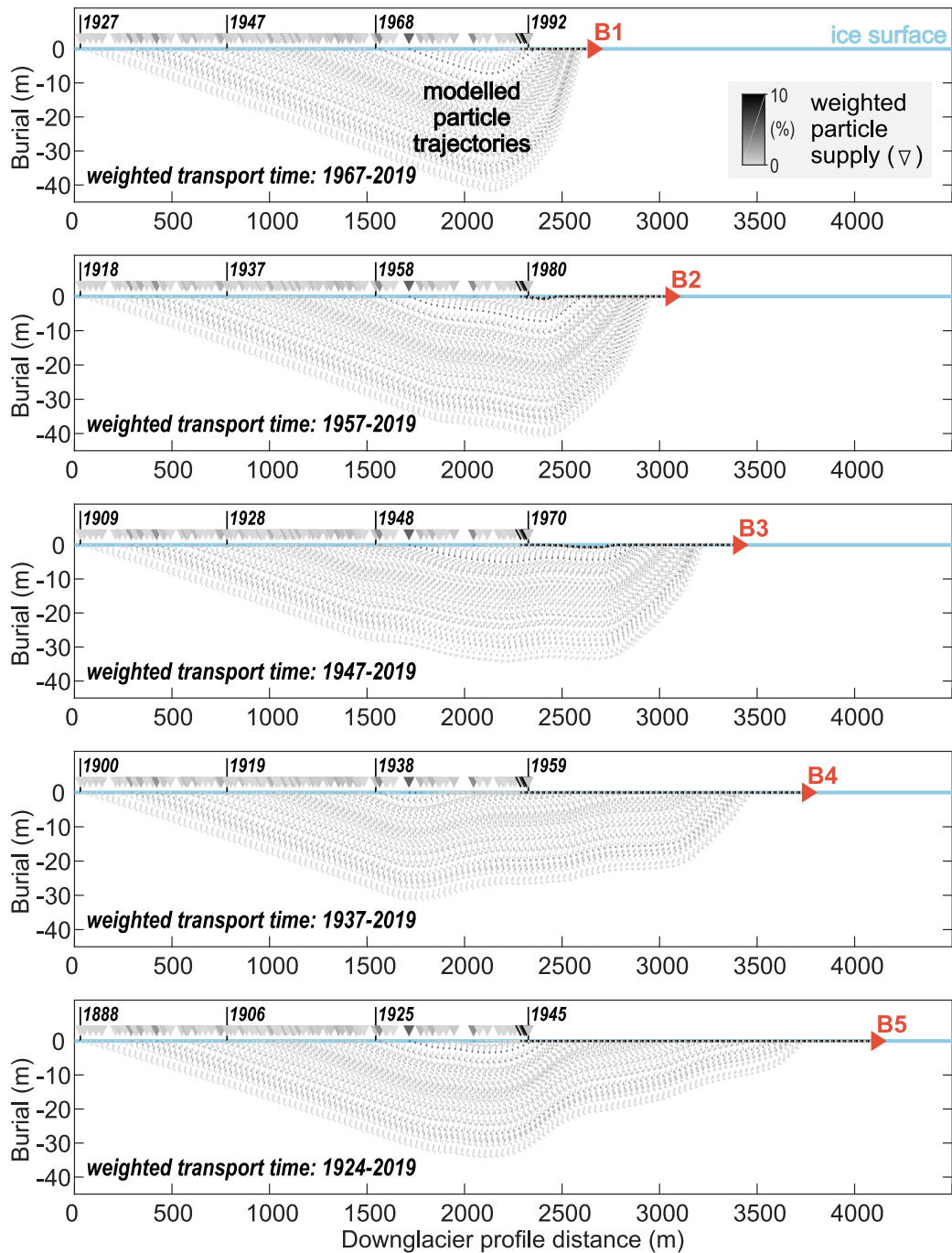
Figure S3: Modelled debris particle trajectories indicating the mode of downglacier particle transport from source rockwalls to sample locations B1-B5 at Glacier du Brenay. Shown are all trajectories of particles deposited along the first ~2.3 km of the downglacier profile that arrive at the ice surface and downglacier distance of a sample's location in 2019. For reference, start years of four trajectories are given. The burial depth indicates whether a particle was transported within the ice (englacially; burial depth <0 m) and shielded from cosmic radiation, or on the ice surface (supraglacially; burial depth = 0 m) and exposed to cosmic radiation. Graded colours indicate the percentage debris particle supply along the first ~2.3 km profile distance (see also Fig. S2b) and the weight of its corresponding trajectory, used to estimate a weighted time of downglacier particle transport.
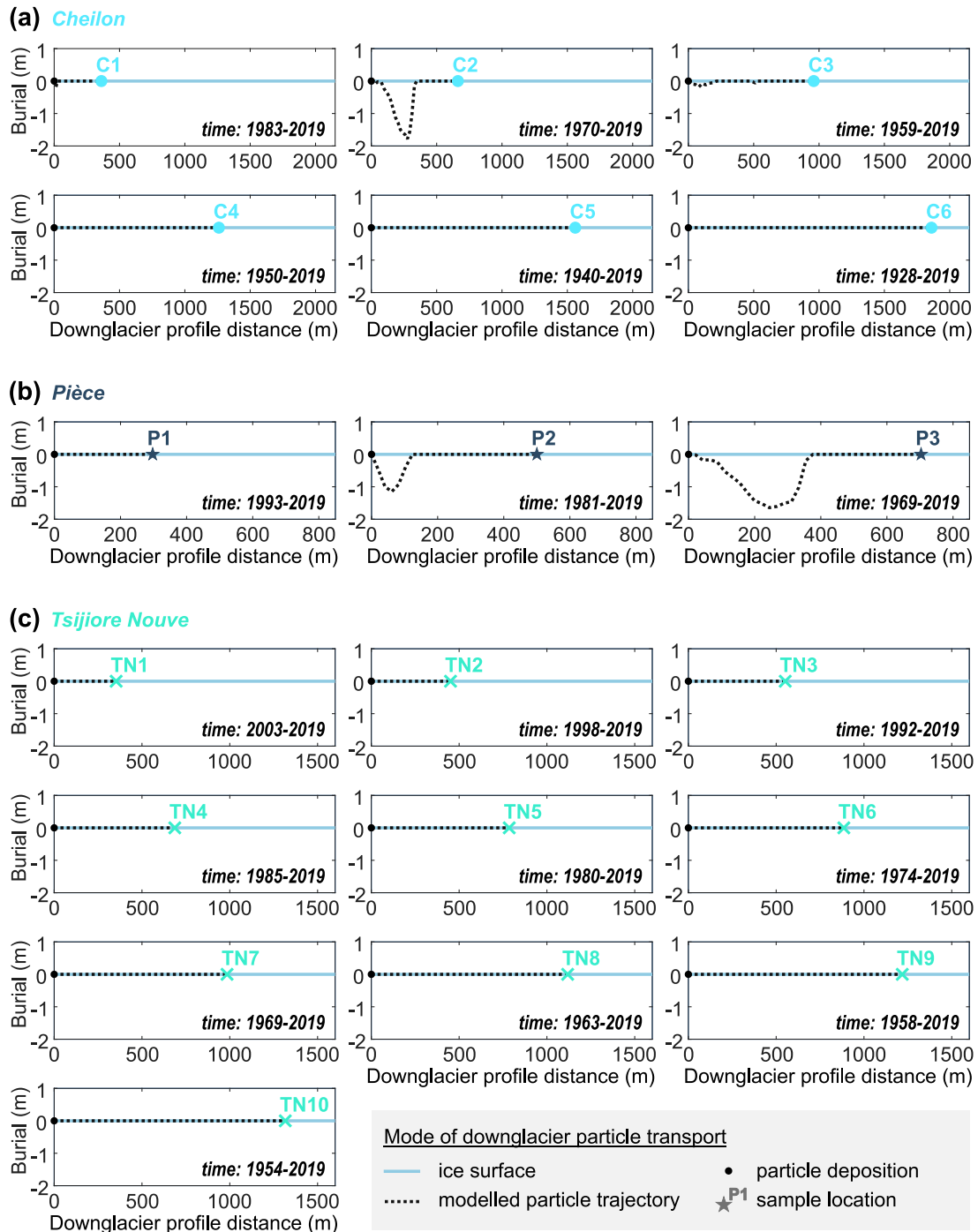
Figure S4: Modelled debris particle trajectories indicating the mode of downglacier particle transport from source rockwalls to sample locations at (a) Glacier de Cheilon, (b) Glacier de Pièce, and (c) Glacier de Tsijiore Nouve. Note that each graph stands for an individual sample. Shown is the burial depth of particles, which indicates whether a particle was transported within the ice (englacially; burial depth <0 m) and shielded from cosmic radiation, or on the ice surface (supraglacially; burial depth = 0 m) and exposed to cosmic radiation. A particle's transport begins at the ice surface and profile head at the time as indicated and ends at the ice surface and downglacier distance of a sample's location in 2019.
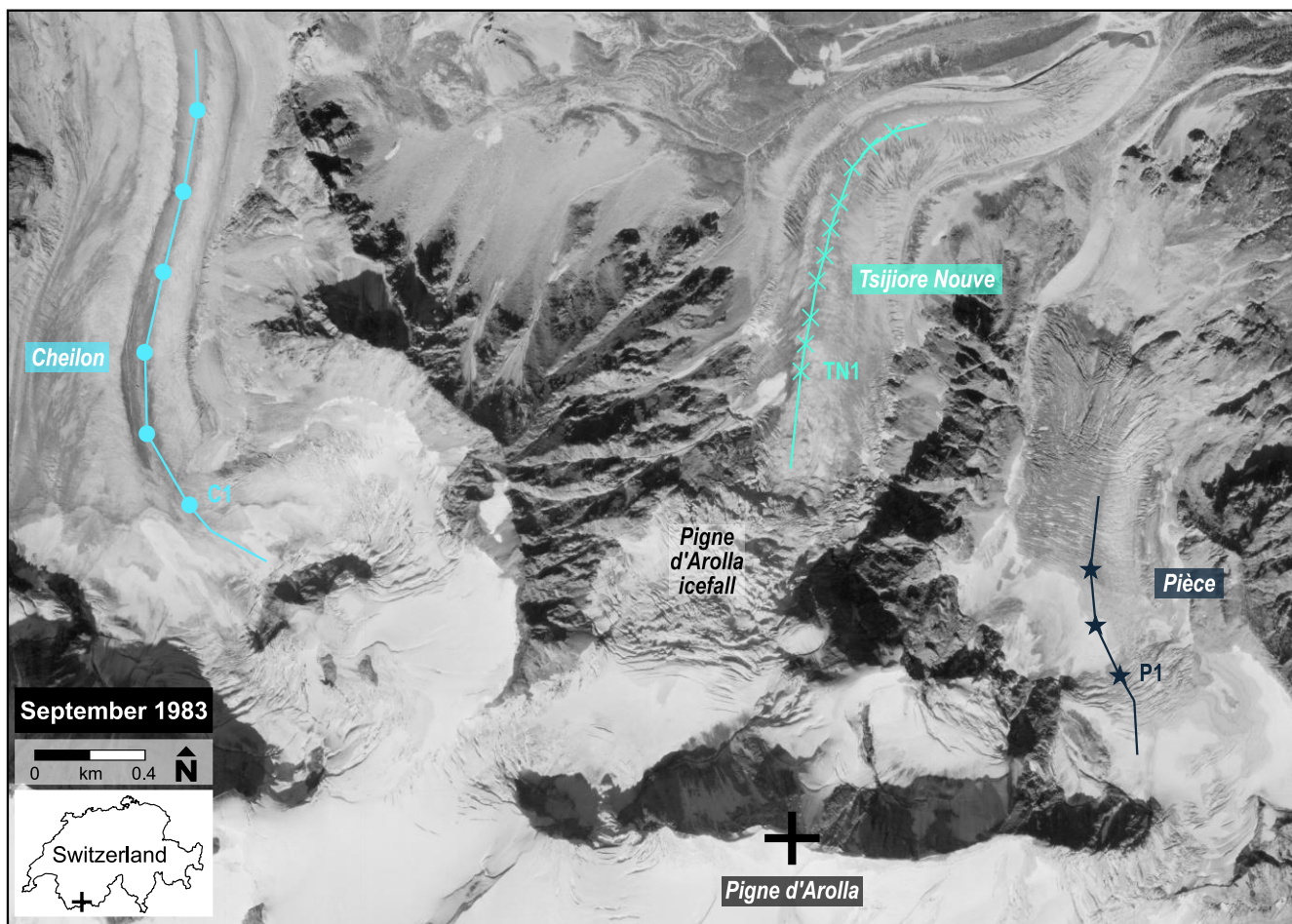
Figure S5: Orthoimage from 1983 indicating englacial debris transport close to the source rockwalls of Glacier de Cheilon and Glacier de Pièce as well as close to the base of the Pigne d'Arolla icefall at Glacier de Tsijiore Nouve. For reference, the respective medial moraine profiles and 2019 sample locations are indicated. The image excerpt is based on aerial images taken in September 1983 (orthoimage by swisstopo, 2022).
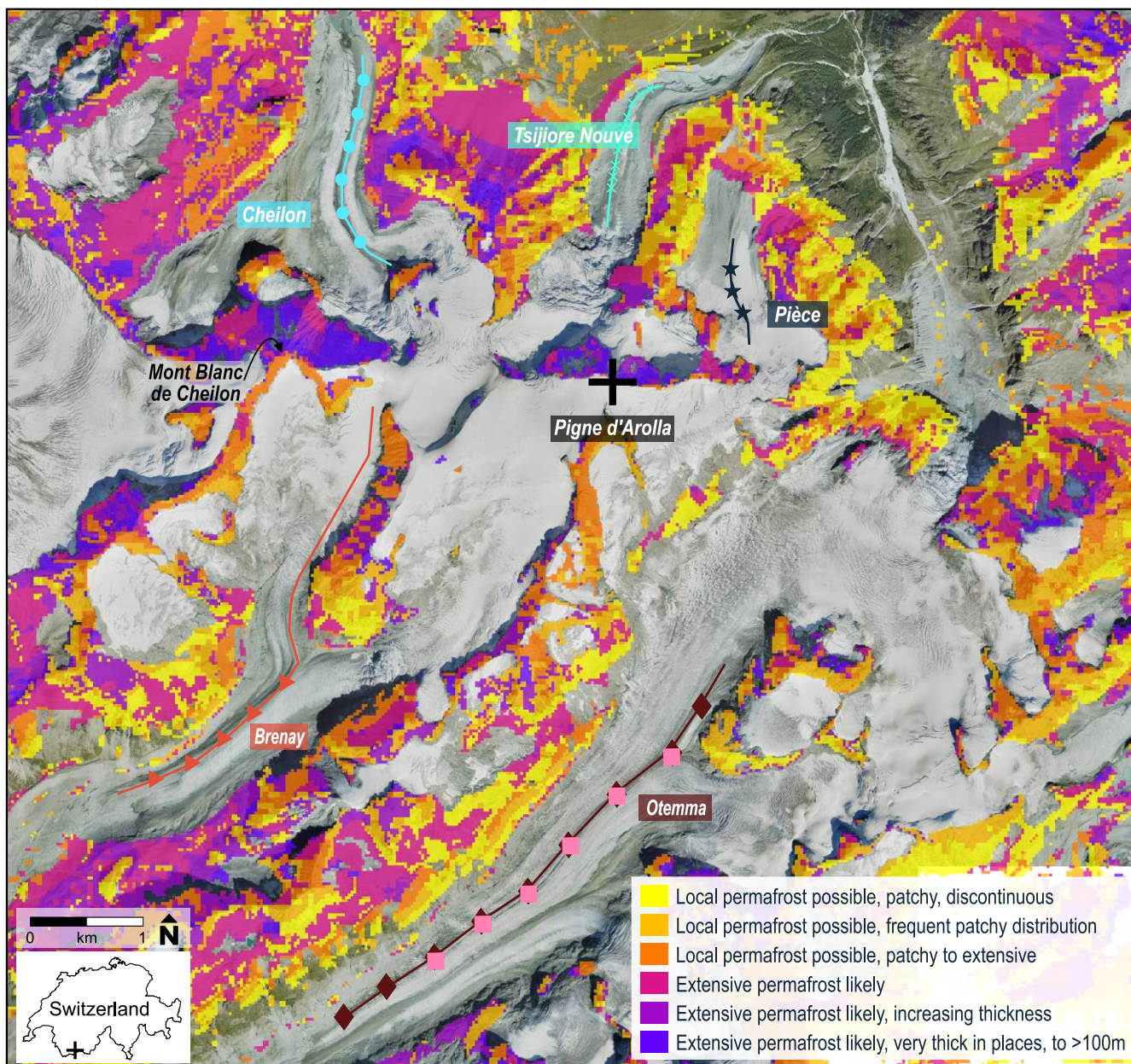
Figure S6: Permafrost distribution map showing the potential zone of modelled mountain permafrost across ice-free rockwalls and slopes in the area around Pigne d'Arolla. For reference, the respective medial moraine profiles and 2019 sample locations of Glacier du Brenay, Glacier de Cheilon, Glacier d'Otemma, Glacier de Pièce, and Glacier de Tsijiore Nouve are indicated. Note the extensive permafrost occurrence at the north faces of the east-west trending ridgeline between Pigne d'Arolla and Mont Blanc de Cheilon compared to the patchier permafrost occurrence to the south (potential permafrost distribution map by BAFU, 2005; orthoimage by swisstopo, 2022).

2 Supplementary Table S1

Table S1: Comparison of model results for downglacier debris particle transport at Glacier du Brenay, Glacier de Cheilon, Glacier de Pièce and Glacier de Tsijiore Nouve, using different glacier surface velocity projections into the past for which we lack boulder tracking data. Listed are the sample ages, the additional ^{10}Be accumulation ($[^{10}$Be$]_{transport}$), and the transport-corrected apparent rockwall erosion rates, based on (1) the velocity projections used in the study, as well as (2) half and (3) twice the velocity assumptions made. Note that the age estimates for the slower/faster glacier surface velocities largely differ by <5 years, except for few samples at Glacier de Cheilon where age differences with up to 14 years are still relatively small and do not affect our findings. The data were computed using the simple 1-D particle trajectory model by Wetterauer et al. (2022b) and, except for the glacier surface velocities, settings/calculations were kept as described in the study.

	Past velocity projections used			1/2× past velocity projections			2× past velocity projections		
	Age	$[^{10}$Be$]_{transport}$ $\times 10^3$	App. erosion rate (transport-corr.)	Age	$[^{10}$Be$]_{transport}$ $\times 10^3$	App. erosion rate (transport-corr.)	Age	$[^{10}$Be$]_{transport}$ $\times 10^3$	App. erosion rate (transport-corr.)
Sample	(yrs)	(atoms g^{-1})	(mm yr^{-1})	(yrs)	(atoms g^{-1})	(mm yr^{-1})	(yrs)	(atoms g^{-1})	(mm yr^{-1})
Glacier du Brenay									
B1	52	0.7	1.0	53	0.7	1.0	52	0.7	1.0
B2	63	0.9	0.7	63	0.8	0.7	62	0.9	0.7
B3	72	1.1	0.7	73	1.1	0.7	70	1.1	0.7
B4	83	1.5	0.8	84	1.5	0.8	80	1.6	0.8
B5	96	1.9	0.7	98	1.9	0.7	92	1.9	0.7
Glacier de Cheilon									
C1	36	1.0	5.1	36	1.0	5.1	36	1.0	5.1
C2	50	1.3	8.9	51	1.3	9.1	48	1.2	8.6
C3	61	1.7	4.5	65	1.8	4.7	55	1.6	4.4
C4	70	2.0	7.6	77	2.2	8.3	62	1.8	7.0
C5	80	2.3	36.7	90	2.5	87.5	70	2.0	23.2
C6	92	2.6	10.0	105	2.6	10.3	78	2.2	8.2
Glacier de Pièce									
P1	27	0.8	5.5	27	0.8	5.5	27	0.8	5.5
P2	39	1.0	5.9	39	1.0	5.9	39	1.0	5.9
P3	50	1.2	7.6	51	1.3	7.7	49	1.2	7.4
Glacier de Tsijiore Nouve									
TN1	16	0.4	10.6	16	0.4	10.6	16	0.4	10.6
TN2	21	0.5	12.7	21	0.5	12.7	21	0.5	12.7
TN3	27	0.6	18.7	27	0.6	18.7	27	0.6	18.7
TN4	34	0.8	15.6	34	0.8	15.6	34	0.8	15.6
TN5	40	0.9	21.3	40	0.9	21.3	40	0.9	21.3
TN6	45	1.0	7.4	45	1.0	7.4	45	1.0	7.4
TN7	50	1.1	15.1	50	1.1	15.1	50	1.1	15.1
TN8	56	1.3	9.3	56	1.3	9.3	56	1.3	9.3
TN9	61	1.4	34.5	61	1.4	34.5	60	1.4	33.2
TN10	65	1.5	18.9	66	1.5	19.3	65	1.4	18.7

3 References

Bundesamt für Umwelt BAFU: Hinweiskarte der potenziellen Permafrostverbreitung, https://map.geo.admin.ch, last access: 14 November 2022, 2005.

Linsbauer, A., Huss, M., Hodel, E., Bauder, A., Fischer, M., Weidmann, Y., Bärtschi, H., and Schmassmann, E.: The new Swiss Glacier Inventory SGI2016: from a topographical to a glaciological dataset, Front. Earth Sci., 9, 1-22, https://doi.org/10.3389/feart.2021.704189, 2021.

Maisch, M., Wipf, A., Denneler, B., Battaglia, J., and Benz, C.: Die Gletscher der Schweizer Alpen: Gletscherhochstand 1850, Aktuelle Vergletscherung, Gletscherschwund-Szenarien, (Schlussbericht NFP 31), 2. Auflage. vdf Hochschulverlag an der ETH Zürich, 373 pp., 2000; & Paul, F.: The new Swiss glacier inventory 2000 - application of remote sensing and GIS, PhD Thesis, Department of Geography, University of Zurich, Schriftenreihe Physische Geographie, 52, 210 pp, 2004.

Müller, F., Caflisch, T., and Müller, G.: Firn und Eis der Schweizer Alpen (Gletscherinventar), Publ. Nr. 57/57a. Geographisches Institut, ETH Zürich, 2 Vols., 1976; & Maisch, M., Wipf, A., Denneler, B., Battaglia, J., and Benz, C.: Die Gletscher der Schweizer Alpen: Gletscherhochstand 1850, Aktuelle Vergletscherung, Gletscherschwund-Szenarien, (Schlussbericht NFP 31), 2. Auflage. vdf Hochschulverlag an der ETH Zürich, 373 pp., 2000; & Paul, F.: The new Swiss glacier inventory 2000 - application of remote sensing and GIS, PhD Thesis, Department of Geography, University of Zurich, Schriftenreihe Physische Geographie, 52, 210 pp, 2004.

Swisstopo: Federal Office of Topography swisstopo, https://map.geo.admin.ch, last access: 14 November 2022.

Wetterauer, K., Scherler, D., Anderson, L.S., and Wittmann, H.: Sample and modelling data for cosmogenic 10Be in medial moraine debris of Glacier d'Otemma, Switzerland, GFZ Data Services, https://doi.org/10.5880/GFZ.3.3.2021.007, 2022b.